Australian Earthquake Engineering Society
2022 National Conference, 24-25 November 2022
Mount Macedon, Victoria, Australia

Updating the Somerville et al. (2009) Ground Motion Model for Cratonic Australia Using Broadband Ground Motion Simulations of Recently Recorded Cratonic Region Earthquakes

Jeff Bayless[1], Paul Somerville[1], Scott Condon[1], Hong Kie Thio,[1] Hadi Ghasemi[2], Trevor Allen[2]

1. AECOM, 300 South Grand Ave, Los Angeles, CA 90071, United States of America

2. Geoscience Australia, Box 378 Canberra ACT 2601, Australia

Abstract

This paper describes the ongoing update of the Somerville et al. (2009; Sea09 hereinafter) Cratonic ground motion model, using broadband strong motion simulations to account for earthquake source and crustal structure properties of Australia. The simulations are validated with new data recorded in Cratonic Australia (provided by Geoscience Australia; Allen and Ghasemi, 2020) and utilise contemporary methods (Graves and Pitarka, 2015; GP15).

Sea09 observed large R_g waves both in recordings and simulations of very shallow Cratonic earthquakes, explained by a shallow low velocity layer in the crust. We develop a new 1D seismic velocity model, consistent with that of Sea09 and representative of Cratonic Australia, using the Australian Seismological Reference Model (Salmon et al., 2013) and calculate theoretical Green's Functions for use in the simulations.

Twelve earthquakes are identified as strong candidates for calibration and validation of the GP15 simulations. The simulations are validated by comparing attenuation, goodness of fit, and spectral shapes. Final selection of GP15 source and attenuation parameters will be based on these validations. We will then use these parameters in a large set of ground motion simulations, and finally update Sea09 based on those simulations.

Keywords: Ground motion models, ground motion simulations, validation, Cratonic regions

1 Introduction

This paper describes the ongoing update of the Sea09 ground motion model for Cratonic earthquakes in Australia. Both Sea09 and the updated model are for the horizontal median (RotD50) component of 5% damped pseudo-spectral acceleration.

The original Sea09 models for Cratonic and non-Cratonic Australia were based on ground motion simulations, and then checked for consistency with the recorded ground motions of the moment magnitude (Mw, or **M**) 4.47 Thompson Reservoir earthquake of 1996, which occurred in non-Cratonic southeastern Australia. In the course of the National Seismic Hazard Assessment (NSHA18; Allen et al., 2018), Geoscience Australia assessed the performance of

existing ground motion models in predicting recorded ground motions in Australia (Ghasemi and Allen, 2018). They demonstrated that Sea09 could be improved by taking advantage of ground motions recorded in the past decade-plus.

The update of Sea09 involves the following five stages. The first two stages are summarised in this paper and the remaining stages will be completed in due course:

Stage 1: Data Collection and Processing. The database of recorded ground motions, described in Section 3, will be used to constrain the empirical model, and select events from the database will be used to validate the simulations.

Stage 2: Simulations of Recorded Earthquakes. Simulations are undertaken to validate the simulation methodology (and its key parameters, described in Section 4) using well-recorded Cratonic-region earthquakes. A selection of these results is provided in Section 5.

Stage 3: Forward Simulations. Upon completion of the validation stage, we will perform a suite of simulations for scenario earthquakes up to **M**7.5 and for rupture distances up to 600 km.

Stage 4: Base Ground Motion Model Regression. The databases of response spectra from recorded earthquakes and the forward simulations will be combined, and a nonlinear mixed effects regression using the unmodified Sea09 model functional form will be used to determine updated model coefficients.

Stage 5: Model Refinement and Comparison. Additional model features will be implemented, such as hanging wall effects, Vs30 scaling, and source-depth scaling. We will test the scaling of individual model components (Vs30, attenuation, magnitude scaling) and compare with the Sea09 model and with other existing models. Finally, a model for the aleatory variability will be developed.

2 Review of Somerville et al. (2009) Model

The Sea09 ground motion models for Australia were developed under contract to Geoscience Australia (Somerville et al., 2009). Given the sparsity of recorded strong motion data in Australia, Sea09 used a broadband strong motion simulation procedure to account for the known earthquake source and crustal structure properties in Cratonic and Non-Cratonic Australia. The Sea09 ground motion model consists of separate Cratonic and Non-Cratonic models representing different shallow crustal structure and seismic wave propagation characteristics (Somerville and Ni, 2010). Sea09 developed and used seismic velocity models for the Perth Basin / Yilgarn Craton region and for the Sydney Basin / Lachlan Fold Belt region in the simulation of earthquake ground motions. Finite fault rupture models were derived for the 1968 Meckering and 1988 Tennant Creek earthquakes through the inversion of teleseismic waves and geodetic data. The rupture models of these earthquakes and other data were used to derive earthquake source models for the strong motion simulations. Finally, the ground motion models for response spectral acceleration were derived from these simulations.

Sea09 compared their Cratonic model to others and found that it was more similar to the model developed using Yilgarn Craton data by Liang et al. (2008), and less similar to the models for stable regions of eastern North America by Toro et al. (1997) and Atkinson and Boore (2006). In Sea09, the very shallow earthquakes and the shallow low velocity layer in the crust in the Cratonic model give rise to large R_g waves that are observed both in the recordings and the simulations. These produce large peak velocities in the records and give rise to a peak in the ground motion response spectrum at a period of about 1.5 seconds.

3 Ground Motion Data

Geoscience Australia (Allen and Ghasemi, 2020) provided instrument corrected recordings for events occurring within Cratonic regions, a subset of which we select to be used in the Sea09 update. Additional waveform data are collected from IRIS (https://ds.iris.edu/wilber3/) and processed to remove instrument responses. To create the waveform database, we removed events with **M** less than 3.0, recordings with distance greater than 600 km, and recordings that have been clipped, have poor signal to noise ratio, or contain artifacts. Recordings without both orthogonal horizontal components are also removed. These actions result in 536, homogeneously processed, ground motion records from 83 events recorded by 143 unique stations, as mapped in Figure 1.

The recorded ground motions used for refining the ground motion model are shown in Figure 2, which displays moment magnitude versus epicentral distance and moment magnitude versus number of recordings per event. There are three earthquakes with more than 80 recorded ground motions, these are the **M**4.27 on 2019 May 30, the **M**4.87 on 2019 May 5, and the **M**4.99 on 2019 August 1. These three earthquakes were located within the Northern Australian Craton (Figure 1) and recorded by the temporary AusARRAY deployment (Gorbatov et al., 2020). The remaining 80 earthquakes in the database have fewer than 10 recordings. There are 35 total events with $\mathbf{M} \geq 4.0$ and 32 events with $3.5 \leq \mathbf{M} < 4.0$.

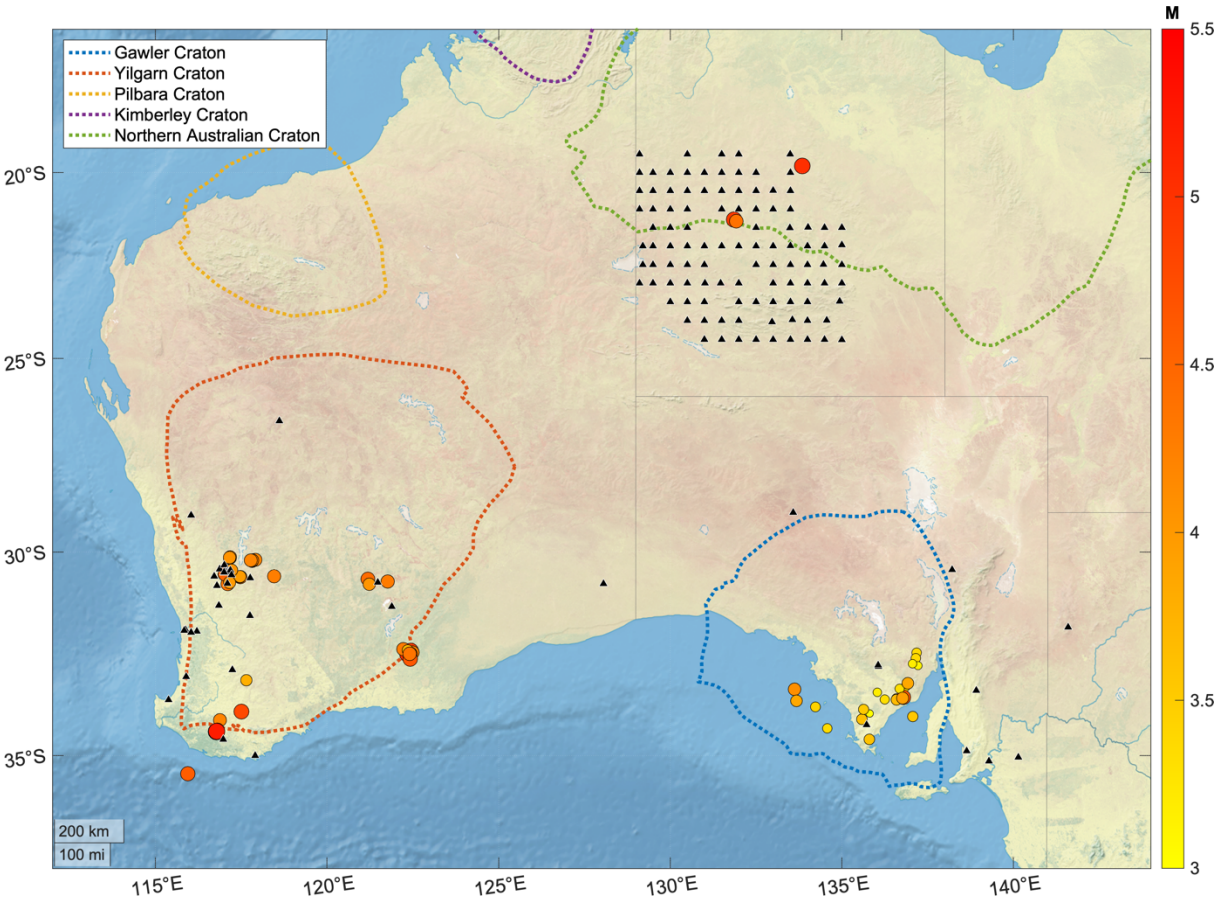

Figure 1. A map of Cratonic domain earthquakes (circles) and recording stations (triangles) with Cratonic domain boundaries from NSHA18 (Clark et al., 2012).

The 5% damped, horizontal component pseudo-spectral accelerations (RotD50) are calculated from two-component band-passed acceleration time histories using the pyRotd python library (Kottke, 2018). Spectral accelerations, in units of gravity, are calculated for oscillatory periods between 0.001 and 10.0 seconds. Approximate finite-fault distances are

calculated using PS2FF, a python software package, which converts epicentral distances (R_{epi}) to Joyner-Boore (R_{jb}) and closest distances to rupture (R_{rup}) (Thompson and Worden, 2017).

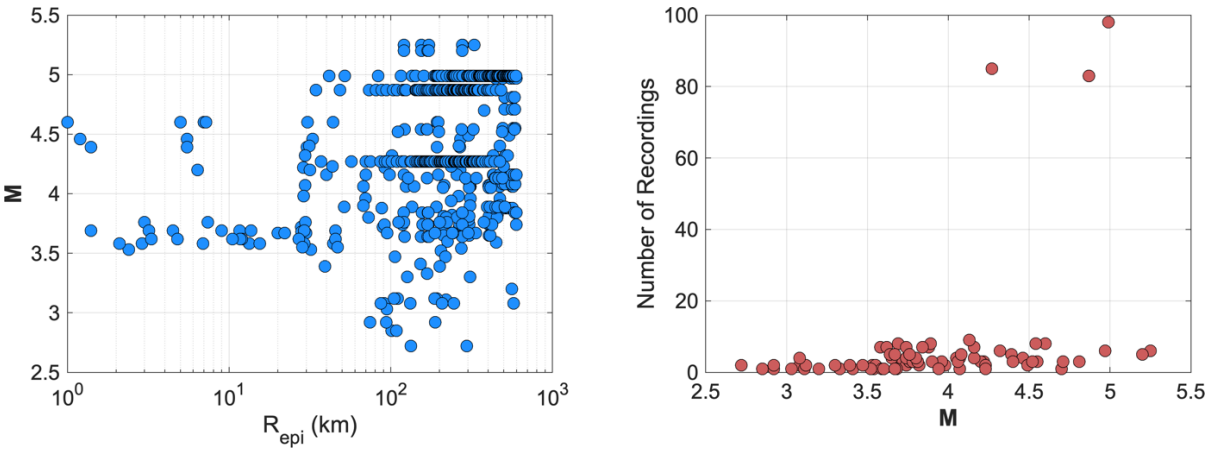

Figure 2. Left: Magnitude versus epicentral distance pairs of the Cratonic regions database obtained from IRIS and Geoscience Australia (Allen and Ghasemi, 2020). Right: The number of ground motion recordings per event versus magnitude.

The database shown in Figures 1 and 2 will be used for constraining the Sea09 update. As described above, this database will be supplemented with simulations. For the purposes of validating the simulations, we identified the 12 earthquakes listed in Table 1 as strong candidates. The first three listed are located within the Northern Australian Craton and have more than 80 recorded ground motions. The next six in the list are located within the Yilgarn Craton and have at least five recordings each, to use in the validation. The final three earthquakes are located in the Gawler Craton and have five recordings each.

Some of the hypocentral depth values provided by Geoscience Australia are provisional, unless noted otherwise in Table 1. These provisional depths are generally poorly constrained and need to be reviewed. AECOM are revising these depths by applying the cut-and-paste method (Tan, 2006; Zhao and Helmberger, 1994) to determine source parameters.

Table 1. The recorded earthquakes used in calibration and validation of the simulations.

EQID	Mw	Date	Epicenter Longitude (deg)	Epicenter Latitude (deg)	Hypocenter Depth (km)	Region	No. of Usable 2-component Recordings
61	4.99	2019-08-01	133.849	-19.822	1.9^	Northern Aus Craton	98
59	4.87	2019-05-30	131.85876	-21.28147	10*	Northern Aus Craton	83
60	4.27	2019-05-30	131.92337	-21.32752	10*	Northern Aus Craton	85
58	5.2	2018-11-08	116.78733	-34.42316	3*	Yilgarn Craton	5
53	5.25	2018-09-16	116.78	-34.43	0*	Yilgarn Craton	6
44	4.97	2016-07-08	122.346	-32.541	0*	Yilgarn Craton	6
13	4.6	2002-03-30	117.049	-30.519	0.8	Yilgarn Craton	8
55	4.54	2018-10-12	116.79882	-34.39522	5.8*	Yilgarn Craton	8
49	4.13	2017-01-03	118.455	-30.609	10*	Yilgarn Craton	9
72	4.81	2010-06-05	136.796	-33.5949	24	Gawler Craton	5
82	3.86	2018-07-01	136.7729	-33.618	26	Gawler Craton	5
83	3.76	2018-11-21	136.923	-33.2585	38	Gawler Craton	5

** Provisional hypocentral depth values from Allen and Ghasemi (2020)*

^ Depth from Shea and Barnhart (2022)

4 Simulation Framework

4.1 Method Overview

We use the hybrid broadband ground motion simulation methodology of Graves and Pitarka (2015; 2014; 2010; 2004; GP15) as implemented on the Southern California Earthquake Center Broadband Platform, version 19.8 (SCEC BBP; Maechling et al., 2015), which was the latest BBP version release at the time this work began. The GP15 method combines a deterministic approach at low frequencies (f<1 Hz) with a semistochastic approach at high frequencies (f>1 Hz), where the broadband (0-10 Hz) response is obtained by summing the separate responses in the time domain using matched filters centred at 1 Hz. In GP15 the fault rupture is represented kinematically and incorporates spatial heterogeneity in slip, rupture speed, and rise time by discretizing an extended finite-fault into a number of smaller subfaults. The GP15 prescribed slip distribution is constrained to follow an inverse wavenumber-squared fall-off and the average rupture speed is set at a fraction of the local shear-wave velocity, which is then adjusted such that the rupture propagates faster in regions of high slip and slower in regions of low slip. At low frequencies (f<1 Hz), the GP15 methodology contains a theoretically rigorous representation of fault rupture and wave propagation effects, and attempts to reproduce recorded ground motion waveforms and amplitudes by summing the response for many point sources distributed across each subfault. At high frequencies (f>1 Hz), GP15 uses a stochastic representation of source radiation, which is combined with a simplified theoretical representation of wave propagation and scattering effects for each subfault.

Graves and Pitarka (2015) extended their broadband simulation method from active region/crustal earthquakes to earthquakes in stable continental regions based on findings from Somerville et al. (2009), Leonard (2010), Beresnev and Atkinson (2002), and with calibration using three eastern North America earthquakes. The modifications included: increasing the average rise time, reducing the average corner frequency, increasing the high frequency stress parameter, using the Leonard (2010) magnitude-area scaling relations, changing the high frequency attenuation (through kappa and Q models), changing the background rupture speed, and removing the shallow and deep weak zones from the rupture characterization (Graves and Pitarka, 2015).

In our Cratonic region earthquake simulations, we began by using the recommendations from Graves and Pitarka (2015) and took a trial-and-error approach to refine the parameters based on the simulation and validation of earthquakes recorded in Australia (Section 5). A summary of the final parameters and values required by the BBP v19.8 implementation of GP15 will be provided upon completion of the Sea09 update. Additional requirements to perform a simulation are the seismic velocity model and 1D Green's functions, the kinematic source description, and the station information and site response. These are described in the following sections.

4.2 Seismic Velocity Model

This section describes the 1D velocity model developed for use in the simulations. The Australian Seismological Reference Model (AuSREM; Salmon et al., 2013) is utilised. AuSREM is a 3D grid based crustal structure model (P wave speed, S wave speed, density and depths of major boundaries) with a 0.5-degree sampling in latitude and longitude, so that properties can be extracted and interpolated at any point in the country. We extract profiles within the Yilgarn and Gawler Cratons at 2-degree intervals in latitude and longitude, and outside of these Cratons in southeast Australia. These profiles are very similar at depths below about 5 km. In the 1-5 km depth range, we find significant differences between the Cratonic and Non-Cratonic profiles. Based on these findings, we develop a representative AuSREM

Cratonic seismic velocity model based on the average of the profiles within the Yilgarn and Gawler cratons, and a representative Non-Cratonic model based on the average of the extracted profiles in southeast Australia. Below 5 km depth these profiles are identical. Above 1 km depth, the models are tapered to yield reference Vs30 values of 2,000 m/s and 760 m/s for the Cratonic and Non-Cratonic regions, respectively. The reference Vs30 value of 760 m/s is a standard velocity for representing firm rock site conditions and is used by the NSHA18, the U.S. Geological Survey, and others (Allen et al., 2018; Peterson et al., 2020). The reference Vs30 value of 2,000 m/s was selected for Cratonic regions based on the Goulet et al. (2021) methodology, which used a value of 3,000 m/s for the stable continental eastern United States to represent very hard rock (VHR). We have assumed that 2,000 m/s also represents VHR conditions and selected this value because it better represents the values measured in practice at VHR sites, and because the difference in site amplification between the 2,000 and 3,000 m/s site conditions is relatively small and not sensitive to the specific velocity profiles (Boore and Campbell, 2017). These reference values represent the site condition for which ground motions will be predicted by the base ground motion model, and to the condition which site amplification factors will be applied (described further in Section 4.3).

The velocity models developed in Sea09 are similar to the AuSREM models at depth, with slightly lower velocities at all depths in Sea09. To develop the final seismic velocity models, the mean of the AuSREM representative models and the Sea09 models is taken, and this mean model is down-sampled to a serviceable number of layers (16 layers for Cratonic and 22 for Non-Cratonic). The final models are shown in Figure 3 and the Cratonic model is listed in Table 2.

The Cratonic seismic velocity model is used to calculate theoretical Green's functions (GFs) including anelastic attenuation, computed using the Zhu and Rivera (2002) frequency-wavenumber technique. The GFs contain the full theoretical waveform response from zero to several Hz. The GFs are computed for three fundamental fault orientations (SS, DS, DD), from which any arbitrary faulting mechanism can be computed using a linear combination of the fundamental fault response. We compute a database of GFs for the Cratonic velocity model and for source depths ranging from 0-30 km and source-site distances ranging from 0-600 km.

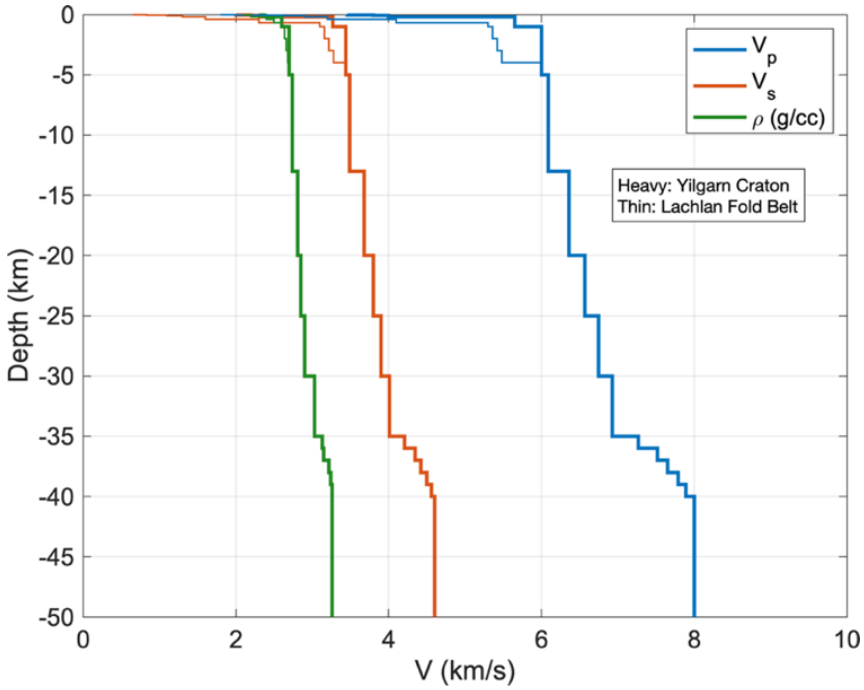

Figure 3. The Cratonic (heavy lines) and Non-Cratonic (thin lines) seismic velocity models.

Table 2. The Cratonic region seismic velocity model.

Layer Thickness (km)	Depth to Top of Layer (km)	Vp (km/s)	Vs (km/s)	Density (g/cc)	Qp	Qs
0.03	0.0	3.460	2.000	2.300	200.000	100.000
0.04	0.03	3.800	2.200	2.360	220.000	110.000
0.13	0.07	4.000	2.310	2.390	231.000	115.500
0.8	0.2	5.650	3.270	2.600	327.000	163.500
4	1	6.003	3.442	2.705	344.200	172.100
8	5	6.088	3.494	2.736	349.390	174.700
7	13	6.361	3.676	2.806	367.600	183.800
5	20	6.569	3.797	2.848	379.650	189.830
5	25	6.745	3.897	2.901	389.740	194.870
5	30	6.934	4.010	3.029	400.980	200.490
1	35	7.270	4.206	3.127	420.600	210.300
1	36	7.519	4.348	3.154	434.780	217.390
1	37	7.653	4.424	3.215	442.390	221.200
1	38	7.785	4.500	3.242	450.000	225.000
1	39	7.889	4.562	3.261	456.150	228.080
999	40	8.000	4.600	3.260	460.000	230.000

4.3 Adjustments for Site Response

The Cratonic region simulations are performed using the GFs with the Vs30 = 2,000 m/s reference condition. In the validation stages, the simulations need to be compared with recordings, which have varying site conditions and site-specific Vs30 values. Therefore, the simulations need to be adjusted to reflect these site-specific Vs30 conditions. For the Cratonic region simulations, the two-step procedure from NGA-East is adopted (Goulet et al., 2021). The first step in this procedure is to use adjustment factors to convert the simulated ground motions with Vs30 = 2000 m/s to the Vs30 = 760 m/s (firm rock) condition using the Boore and Campbell (2017) and Stewart et al. (2020) models, and the second step is to adjust from the Vs30 = 760 m/s firm rock site condition to the site-specific Vs30 using the Stewart et al. (2020) model. The simulations are adjusted using the best available Vs30 for each site from Allen and Ghasemi (2020).

Future non-Cratonic region simulations will use the GFs with reference value of Vs30 = 760 m/s and will be adjusted to reflect the site-specific Vs30 conditions using the Boore et al. (2014), and Chiou and Youngs (2014) Vs30-scaling models.

5 Selection of Simulation Results

The simulations are performed for the events and recording stations listed in Table 1, using the GP method and with the Green's functions from the seismic velocity model listed in Table 2. The simulation results for the first event in Table 1 (EQID 61) are presented in this paper.

The EQID 61 simulation has magnitude, dimensions, depth, dip angle and average rake angle as listed in Table 3. The AusARRAY sites which recorded the EQID 61 earthquake, shown in Figures 1 and 4, are located near or within the Northern Australian Craton NSHA18 region, and their site conditions are poorly known. The uncertainties in Vs30 values and in the site response adjustments are significant and could be reduced in the future with additional data collection or improved models; these sources of uncertainty were similarly identified and accepted in NGA-East (Goulet et al., 2021).

Table 3. Characteristics of the EQID 61 simulation source model.

Mw	Fault Length (km)	Fault Width (km)	Depth to Top of Rupture (km)	Dip (deg)	Rake (deg)
4.99	2.52	2.5	0.2	45	90

Figure 4 shows the rupture model for this simulation and a map of the source location relative to the recording stations. Figure 5 shows the simulated velocity time series by hypocentral distance for the north-south horizontal component (left) and east-west horizontal component (right).

For a given spectral period and recording station, the residual is defined as the difference between the natural logarithm of the recorded spectral acceleration (data) and the simulated spectral acceleration after correcting for site conditions. Using this formula, negative residuals correspond to simulation over-prediction. Figure 6 shows the distance attenuation of RotD50 spectral acceleration (top) and logarithmic residuals versus distance (bottom) for peak acceleration. Figure 7 shows simulated response spectra at three example recording stations, and compares with the recorded spectra and the median unmodified Sea09 model for this scenario. In the distance attenuation panels, the Sea09 median plus and minus one standard deviation are shown and the circles represent stations inside the Cratonic region boundary, while squares represent stations outside of (but nearby) this boundary.

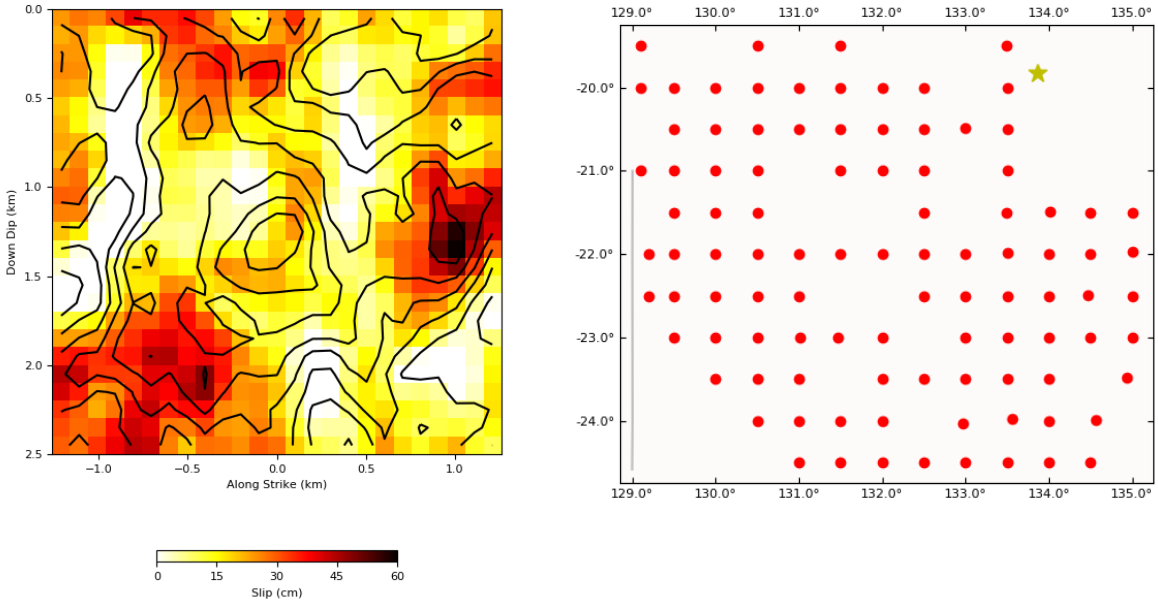

Figure 4. Left: The rupture model for this simulation. Right: A map of the earthquake location (star) and simulation stations (circles).

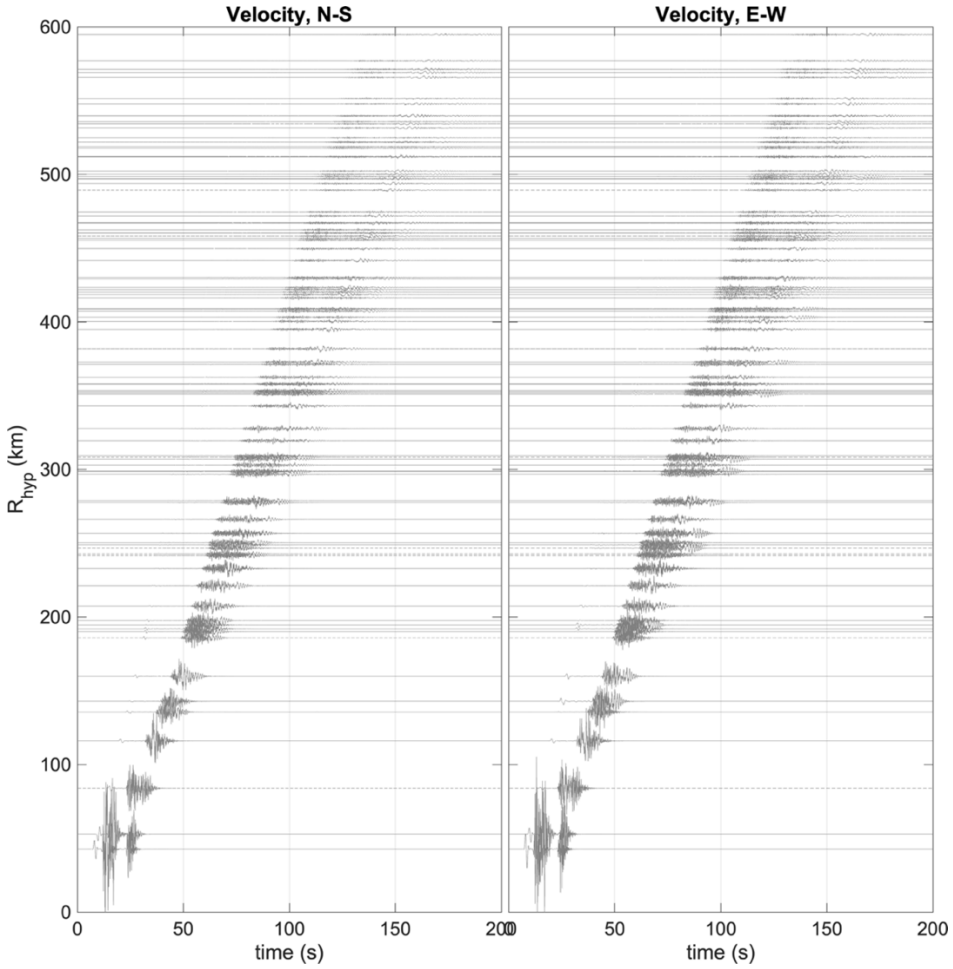

Figure 5. Simulated velocity time series by hypocentral distance for the north-south horizontal component (left) and east-west horizontal component (right).

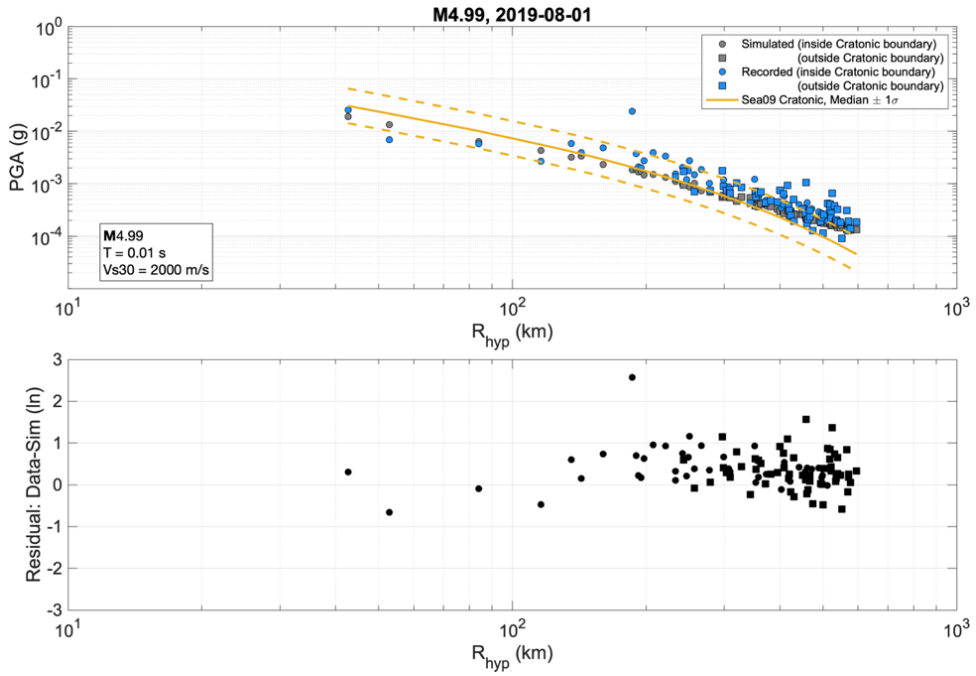

Figure 6. Top: Distance attenuation of PGA for recordings (blue), simulations (grey), and the unmodified Sea09 Cratonic model (yellow). Bottom: Residuals versus distance where the residual is defined as the difference between the natural logarithm of the recorded spectral acceleration (data) and the simulated spectral acceleration.

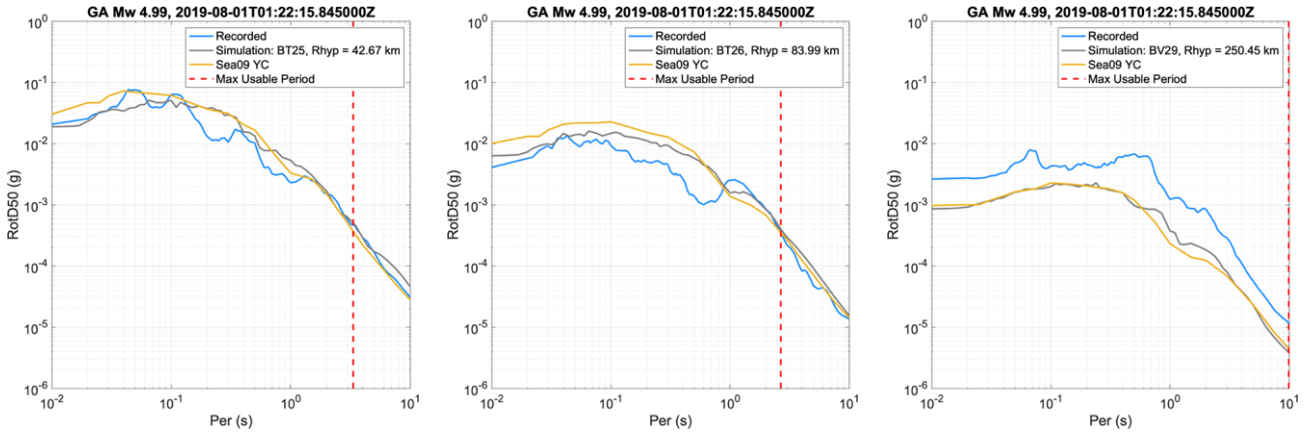

Figure 7. Simulated response spectra at three example recording stations, showing recorded (blue), simulated (grey) and the unmodified Sea09 Cratonic median model (yellow).

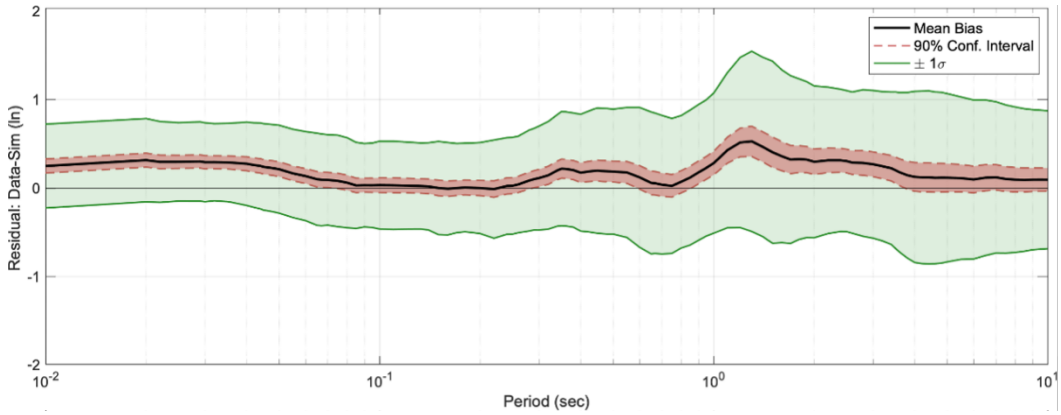

Figure 8. The goodness-of-fit (GOF) summary for this earthquake simulation. The mean bias (black line) is the mean residual calculated from all recording stations for this earthquake. The red shaded area represents the 90% confidence interval in the mean bias and the green shaded area represents +/- 1 standard deviation among the residuals.

Finally, Figure 8 shows the goodness-of-fit (GOF) summary for this earthquake simulation. The GOF is computed for each spectral period. The mean bias (black line) is the mean residual calculated from all recording stations, using the same definition of residual as defined previously. The red shaded area represents the 90% confidence interval in the mean bias and the green shaded area represents +/- 1 standard deviation among the residuals.

6 Future Steps

To complete the update of Sea09, we will complete Stages 3-5 described in the Introduction of this paper: Stage 3 - Forward Simulations, Stage 4 – Base Ground Motion Model Regression, and Stage 5 – Model Refinement and Comparison.

In Stage 3, we will run simulations for the suite of reverse-faulting scenario events listed in Table 4. The rupture dimensions are determined from the Leonard (2010) magnitude-area scaling relations for stable regions. For each scenario in Table 4, we will perform simulations for a range of source depths and for up to five kinematic source realizations. Each scenario has simulation stations oriented in bands around the fault with rupture distances of 5, 10, 15, 20, 30, 40, 50, 60, 70, 80, 90, 100, 150, 200, 300, 400, and 600 km. Each band has at least 20 stations spaced equally around the fault.

In Stage 4, the regression for ground motion model coefficients will be based on the combination of the Stage 3 simulations (Table 4) and the recorded data described in Section

3. Stage 5 will involve the final selection of the functional form of the model. In their review of GMMs for NSHA18, Ghasemi and Allen (2018) found the ground motion models that appear to perform relatively well across all selected periods, tectonic regions, and distance ranges are Allen (2012), Boore et al. (2014), and Chiou and Youngs (2014) models. We will review the functional forms of these three models and find what is common among them and with the Sea09 model. At this stage we will also consider how to model other features such as hanging wall effects, Vs30 scaling, and source depth scaling. We will test the scaling of individual model components (Vs30, attenuation, magnitude scaling) and compare with the Sea09 model and with other existing models. Finally, we will develop a model for the aleatory variability.

Table 4. Source dimensions for the forward simulations.

Mw	Seismic Moment, Mo (dyne-cm)	Cratonic Australia			Non-Cratonic Australia (for reference only)		
		Area (km^2)	Length (km)	Width (km)	Area (km^2)	Length (km)	Width (km)
4.0	$1.12x10^{22}$	0.65	0.64	1.01	1.00	0.71	1.40
4.5	$6.31x10^{22}$	2.04	1.28	1.59	3.16	1.43	2.22
5.0	$3.55x10^{23}$	6.46	2.56	2.52	10.00	2.85	3.51
5.5	$2.0x10^{24}$	20.4	5.1	4.0	31.6	5.7	5.6
6.0	$1.12x10^{25}$	64.6	10.2	6.3	100.0	11.3	8.8
6.5	$6.3x10^{25}$	204.2	20.3	10.1	316.2	22.6	14.0
7.0	$3.55x10^{26}$	645.7	40.5	15.9	1000.0	45.1	22.2
7.5	$2.0x10^{27}$	2041.7	80.9	25.3	3162.3	90.0	35.1

7 Summary

During the NSHA18, Geoscience Australia assessed the performance of existing ground motion models in predicting recorded ground motions in Australia (Ghasemi and Allen, 2018). They showed that Sea09 could be improved by taking advantage of ground motions recorded in the past decade-plus. This paper describes the ongoing update of the Sea09 ground motion model for Cratonic earthquakes in Australia. Both Sea09 and the updated model are for the horizontal median (RotD50) component of 5% damped pseudo-spectral acceleration. The update of the model utilises GP15 broadband strong motion simulations to account for earthquake source and crustal structure properties of Australia. The simulations are validated with new data recorded in Cratonic Australia (Allen and Ghasemi, 2020).

The update of Sea09 involves five stages. The first two stages (data collection and simulation and validation of the recorded earthquake) are summarised in this paper and the remaining stages will be completed in due course. Upon completion, the updated Sea09 model will be based on recorded data and simulations, will include revised coefficients, and will have additional features not in Sea09 such as hanging wall effects, Vs30 scaling, and source depth scaling. The model will include components for median RotD50 and for the aleatory variability.

8 References

Abrahamson, N.A. and W.J. Silva (1997). Empirical response spectral attenuation relations for shallow crustal earthquakes. Seismological Research Letters 68, 94-127.

Abrahamson, N.A. and R.R. Youngs (1992). A stable algorithm for regression analysis using the random effects model. Bull. Seism. Soc. Am. 82, 505-510.

Allen, T.I. (2012). Stochastic ground-motion prediction equations for southeastern Australian earthquakes using updated source and attenuation parameters. Geoscience Australia Record 2012/069.

Allen, T.I. (2018). The 2018 National Seismic Hazard Assessment for Australia: Data package: Maps and grid values. Geoscience Australia record 2018/33. Canberra, ACT, Australia

Allen, T., J. Griffin, M. Leonard, D. Clark and H. Ghasemi (2018). The 2018 National Seismic Hazard Assessment: Model overview. Record 2018/27. Geoscience Australia, Canberra. http://dx.doi.org/10.11636/Record.2018.027

Allen, T. I., Ghasemi, H. (2020). A Ground-Motion Database for Western and Central Australian Earthquakes: Provisional Dataset Prepared for the Seismic Hazard Assessment of the National Radioactive Waste Management Facility. Professional Opinion 2020/xx. Geoscience Australia, Canberra.

Atkinson, G.M. and Boore, D.M. (2006). Earthquake ground-motion prediction equations for eastern North America. Bull. Seism. Soc. Am., 96, 2181-2205.

Beresnev, I. A., and G. M. Atkinson (2002). Source parameters of earthquakes in eastern and western North America based on finite-fault modeling, Bull. Seis. Soc. Am. 92, 695–710.

Boore, D.M., J. P. Stewart, E. Seyhan, and G, M. Atkinson (2014). NGA-West2 Equations for Predicting Response Spectral Accelerations for Shallow Crustal Earthquakes, Earthquake Spectra 30, 1057-1085.

Boore, D.M. and K.W. Campbell (2017). Adjusting Central and Eastern North America Ground-Motion Intensity Measures between Sites with Different Reference-Rock Site Conditions. Bulletin of the Seismological Society of America; 107 (1): 132–148. doi: https://doi.org/10.1785/0120160208

Boore, D. M. (2015). Adjusting ground-motion intensity measures to a reference site for which Vs30 = 3000 m/s, PEER Report 2015/06, Pacific Earthquake Engineering Research Center, University of California, Berkeley, California, 85 pp.

Chiou, B.S.-J. and R.R. Youngs (2014). Update of the Chiou and Youngs NGA Ground Motion Model for Average Horizontal Component of Peak Ground Motion and Response Spectra, Earthquake Spectra 30, 1117-1153.

Clark, D, McPherson, A, Van Dissen, R (2012). Long-term behaviour of Australian stable continental region (SCR) faults. Tectonophysics 566–567: 1–30.

Ghasemi, H. and Allen, T. (2018). Selection and ranking of ground-motion models for the 2018 National Seismic Hazard Assessment of Australia: summary of ground-motion data, methodology and outcomes. Record 2018/29. Geoscience Australia, Canberra.

Graves R. W., Pitarka A. (2004). Broadband time history simulation using a hybrid approach, Proc. 13th World Conf. Earthq. Eng., Vancouver, Canada, paper no. 1098

Graves, R. W., Pitarka, A. (2010). Broadband ground-motion simulation using a hybrid approach, Bull. Seismol. Soc. Am. 100, 2095–2123, doi: 10.1785/0120100057.

Graves R. W., Pitarka A (2015). Refinements to the Graves and Pitarka (2010) Broadband Ground-Motion Simulation Method. Seismological Research Letters; 86 (1): 75–80. doi: https://doi.org/10.1785/0220140101

Gorbatov, A., K. Czarnota, B. Hejrani, M. Haynes, R. Hassan, A. Medlin, J. Zhao, F. Zhang, M. Salmon, H. Tkalcic, H. Yuan, M. Dentith, N. Rawlinson, A. Reading, B. Kennett, C. Bugden, and M. Costelloe (2020). AusArray: quality passive seismic data to underpin updatable national velocity models of the lithosphere; In, doi: 10.11636/135284.

Goulet, C.A, Bozorgnia, Y., Kuehn, N., Al Atik, L., Youngs, R.R., Graves, R.W. and Atkinson G.M. (2021). NGA-East Ground-Motion Characterization Model Part I: Summary of Products and Model Development. Earthquake Spectra, 37(S1): 1231–1282. https://doi.org/10.1177/87552930211018723

Kottke, A. (2018, July 27). arkottke/pyrotd v0.5.4 (Version v0.5.4). Zenodo. http://doi.org/10.5281/zenodo.1322849

Leonard, M. (2010). Earthquake Fault Scaling: Self-Consistent Relating of Rupture Length, Width, Average Displacement, and Moment Release. Bull. Seis. Soc. Am, 100, 1971-88.

Liang, J. Z., Hao, H., Gaull, B. A. and Sinadinovski, C. (2008). Estimation of Strong Ground Motions in Southwest Western Australia with a Combined Green's Function and Stochastic Approach, Journal of Earthquake Engineering, 12:3,382 – 405.

Maechling, P. J., F. Silva, S. Callaghan, and T. H. Jordan (2015). SCEC Broadband Platform: System Architecture and Software Implementation, Seismol. Res. Lett., 86, no. 1

Petersen, M. D., Shumway, A. M., Powers, P. M., Mueller, C. S., Moschetti, M. P., Frankel, A. D., et al. (2020). The 2018 update of the US national seismic hazard model: Overview of model and implications. Earthq. Spectra 36, 5–41. doi:10.1177/8755293019878199

Salmon, M, B. L. N. Kennett, E. Saygin (2013). Australian Seismological Reference Model (AuSREM): crustal component, Geophysical Journal International, Volume 192, Issue 1, January, 2013, Pages 190–206, https://doi.org/10.1093/gji/ggs004

Shea, H. N., and W. D. Barnhart (2022). The Geodetic Centroid (gCent) Catalog: global earthquake monitoring with satellite imaging geodesy, Bull. Seismol. Soc. Am., doi: 10.1785/0120220072.

Somerville, P.G., R.W. Graves, N.F. Collins, S.G. Song, S. Ni and P. Cummins (2009). Source and ground motion models of Australian earthquakes. Proceedings of the 2009 Annual Conference of the Australian Earthquake Engineering Society, Newcastle, Dec 11-13.

Somerville, P. and S. Ni (2010). Contrast in Seismic Wave Propagation and Ground Motion Models between Cratonic and Other Regions of Australia. In Proceedings of the Australian Earthquake Engineering Society, 2010 Conference.

Stewart, J. P., G.A. Parker, G.M. Atkinson, D.M. Boore, Y.M.A. Hashash, and W.J. Silva (2020). Ergodic site amplification model for central and eastern North America. Earthquake Spectra 36 (1), 42-68.

Thompson, E. M., and C. B. Worden (2017). Estimating rupture distances without a rupture, Bulletin of the Seismological Society of America. https://doi.org/10.1785/0120170174.

Tan, Y. (2006) Broadband Waveform Modeling Over a Dense Seismic Network. Dissertation (Ph.D.), California Institute of Technology. doi:10.7907/F4DB-2K48

Toro, G.R., N.A. Abrahamson, and J.F. Schneider (1997). Model of strong ground motions from earthquakes in central and eastern North America: best estimates and uncertainties. Seismological Research Letters, 68(1), 41-57.

Zhao, L. S., and D. V. Helmberger (1994). Source estimation from broadband regional seismograms, Bull. Seismol. Soc. Am., 84, 91–104.

Zhu, L. and L.A. Rivera (2002). A note on the dynamic and static displacements from a point source in multilayered media, GJI, 148:3, 619–627.